REPORT DOCUMENTATION PAGE

AFRL-SR-AR-TR-05-

0115

1. REPORT DATE (DD-MM-YYYY)	2. REPORT TYPE	3. DATES COVERED (From - To)
21-03-05	Final Report	01-01-04 to 12-31-04

4. TITLE AND SUBTITLE

To Investigate the Impact of Tailorable Interface on the Morphology and Performance Characteristics of High Temperature Nanocomposite

5a. CONTRACT NUMBER

5b. GRANT NUMBER
FA9550-04-1-0021

5c. PROGRAM ELEMENT NUMBER

6. AUTHOR(S)

Dharmaraj Raghavan

5d. PROJECT NUMBER

5e. TASK NUMBER

5f. WORK UNIT NUMBER

7. PERFORMING ORGANIZATION NAME(S) AND ADDRESS(ES)

Howard University,
2400 Sixth Street, NW
Washington DC 20059

8. PERFORMING ORGANIZATION REPORT NUMBER

9. SPONSORING / MONITORING AGENCY NAME(S) AND ADDRESS(ES)

USAF,AFRL, AFOSR
4015 Wilson Blvd. Arlington, VA 22203-1954

NL

10. SPONSOR/MONITOR'S ACRONYM(S)

11. SPONSOR/MONITOR'S REPORT NUMBER(S)

12. DISTRIBUTION / AVAILABILITY STATEMENT

Approval for Public Release: Distribution Unlimited

13. SUPPLEMENTARY NOTES

14. ABSTRACT

Considerable research has been conducted in improving the performance characteristics of nanocomposites, relatively few attempts have been made to address the thermal stability of nanocomposite. This research is focused on the preparation of the layered organosilicates with higher thermal stability, which can be used to make high-temperature polymer nanocomposites. Two approaches to formulate layered organosilicates nanocomposites with higher thermal stability were studied.

In the first approach, apophyllite, a pure, natural and commercially-available layered silicate, was treated with 7-octenyltrichlorosilane in order to chemically graft the functional pendent organic group containing a C=C bond. The characterization from Fourier transform infrared (FTIR) spectroscopy, wide-angle x-ray diffraction (WAXD) and thermal gravimetric analysis (TGA) supports that the organic pendant group was successfully covalently grafted in the layered-silicate backbone, and the layered organosilicate is high thermally stable (decomposition temperature: ~430°C). In addition, vinyl ester nanocomposites were formulated and mechanical properties evaluated

In the second approach, a pure, natural and commercially-available layered silicate, was treated with synthesizied imidazolium salts. The nanodispersion of imidazolium treated clay in an epoxy matrix was evaluated qualitatively by X-ray diffraction (XRD), transmission electronic microscopy (TEM), confocal laser microscopy, and laser induced fluorescence spectroscopy. Results from the four complimentary techniques enable the characterization of the clay platelets over several length scales ranging from the micrometer to the nanometer scale. Mechanical property evaluation of the nanocomposites are underway.

15. SUBJECT TERMS

16. SECURITY CLASSIFICATION OF:			17. LIMITATION OF ABSTRACT	18. NUMBER OF PAGES	19a. NAME OF RESPONSIBLE PERSON
a. REPORT	b. ABSTRACT	c. THIS PAGE			Dr. Wayne Patterson
					19b. TELEPHONE NUMBER (include area code) (202)-806-5567

To Investigate the Impact of Tailorable Interface on the Morphology and Performance Characteristics of High Temperature Nanocomposites

D. Raghavan (PI)
Howard University
525 College Street, NW
Department of Chemistry
Washington DC 20059

&

Dr. Chenggang Chen (Collaborator)
University of Dayton Research Institute
300 College Park
Dayton, OH 45469-0168

First Year Progress Report & Second Year Proposal
AFOSR/NL
110 Duncan Avenue, Suite B115
Bowling Air Force Base
Washington, DC 20332-8080

ABSTRACT

Considerable research has been conducted in improving the performance characteristics of nanocomposites, relatively few attempts have been made to address the thermal stability of nanocomposite. This research is focused on the preparation of the layered organosilicates with higher thermal stability, which can be used to make high-temperature polymer nanocomposites. Two approaches to formulate layered organosilicates nanocomposites with higher thermal stability were studied.

In the first approach, apophyllite, a pure, natural and commercially-available layered silicate, was treated with 7-octenyltrichlorosilane in order to chemically graft the functional pendent organic group containing a C=C bond. The characterization from Fourier transform infrared (FTIR) spectroscopy, wide-angle x-ray diffraction (WAXD) and thermal gravimetric analysis (TGA) supports that the organic pendant group was successfully covalently grafted in the layered-silicate backbone, and the layered organosilicate is thermally stable (decomposition temperature: ~430°C). In addition, apophyllite filled vinyl ester composites were formulated and mechanical properties evaluated.

In the second approach, a pure, natural and commercially-available layered silicate, was treated with synthesizied imidazolium salts. ^{1}H NMR and matrix assisted laser desorption/ionization time-of-flight mass spectrometry (MALDI-TOFMS) were used to characterize the imidazolium salts. The nanodispersion of imidazolium treated clay in an epoxy matrix was evaluated qualitatively by X-ray diffraction (XRD), transmission electronic microscopy (TEM), confocal laser microscopy, and laser induced fluorescence spectroscopy. We have demonstrated the applicability of confocal laser microscopy to study the dispersion of clay layers, tagged by a fluorescent dye in the epoxy matrix. XRD and TEM results reveal that the hand mixed nanocomposite has tactoid morphology, while ultrasonicated organoclay (without hydroxyl group) epoxy nanocomposite has intercalated morphology, and an ultrasonicated organoclay (with hydroxyl group) epoxy nanocomposite exhibit a mixed morphology (intercalated structure with exfoliation). Results from the four complimentary techniques enable the characterization of the clay platelets over several length scales ranging from the

length scales ranging from the micrometer to the nanometer scale. Mechanical property evaluation of the nanocomposites are underway.

INTRODUCTION

During the last decade, the area of nanoclay filled polymers has received much attention from both the scientific and technological communities with the expectation that the materials designed will be lighter and more superior than the pristine polymers. In particular, the attractiveness of polymer-clay nanocomposites resides in the potential of adding small amounts of clay platelets to polymeric resin, to dramatically improve mechanical, thermal, barrier, and flame-retardant properties without reducing the transparency of the pristine polymeric material (1-8). Because of the potential benefits of adding inexpensive clay filler to polymer matrix, the automotive and aerospace industries view polymer clay hybrid nanocomposites as the structural materials of the 21st century (9).

Considerable research has been conducted to study the structure-property relationship of organically modified clay/epoxy nanocomposites (10-16). Tsai and Sun (17) modeled the load transfer efficiency in nanocomposites and noted that significant enhancement in reinforcement can be achieved by having the clay platelets well dispersed in the polymer matrix. By ion exchanging Na^{+}, Ca^{+2}, or K^{+} on the clay surface with a long chain cation, attempts have been made to disperse layered particles (organophilic) in polymer matrix (organophobic). Typically nanoclays treated with alkyl ammonium ions, have been used to produce transparent clay-epoxy nanocomposites. The architecture of the alkyl ammonium ion has been commonly chosen so as to improve clay compatibility with a given polymer resin and provide sufficient layer separation for polymer chains to infiltrate. Recently, Vaia et al., (18) investigated the ability of secondary functional groups on the alkylammonium cations to promote intra-gallary polymerization and clay exfoliation. The study found that the presence of hydroxyl groups in the bis(2-hydroxy-ethyl) methyl tallow ammonium cation faciliated clay exfoliation in a diglycidyl ether bisphenol A (DGEBA)/poly(ether amine) epoxy resin. This work clearly demonstrated the desirability of using onium salts having a secondary functional hydroxyl group for clay platelet exfoliation in epoxy matrix. Organic modifiers can participate in the

reaction(s) with resin components and improve the miscibility of the clay with resin. Conceptually, the organic modifiers can assist in polymer network formation, interface reaction and ultimately dictate the final morphology of nanocomposite by providing layer separation.

Another approach to achieving clay platelet dispersion in polymer matrix is to add compatibilizers to enhance the compatibility between polymer and an organoclay (19-21). A compatibilizer containing polar groups can be intercalated between the layers of the clay via strong hydrogen bonding. The compatabilizer weakens the ionic interaction between clay layers. Examples of compatabilizers are maleic anhydride, glycidyl methacrylate, and styrene. The criteria for swelling agent/comaptabilizer selection are based on its miscibility with the polymer and its ability to swell the organically modified clay.

The clay platelet morphology in a polymer matrix can also be altered based on the processing conditions. While there are reports that explore the importance of processing conditions to make exfoliated nanocomposite with thermoplastic matrix, limited work has been done to investigate the importance of processing parameters on exfoliated nanocomposite with thermoset matrix. Mechanical mixing (compounding, sonication, shear) is necessary – and the efficiency of mixing is dependent on the medium viscosity and reactivity. Ultrasound sonication is a form of vibration that provides energy for the nanoclay platelets to escape from the surrounding restraining force. Ultrasound sonication of premixed nanoclay/polymer samples has shown promise in the dispersion or exfoliation of the nanoclay platelets in polymer matrix (22). All these approaches are attractive, and they provide a framework to manipulate the morphology of nanocomposites, so as to achieve optimal properties.

Although factors influencing the morphology of nanocomposite have been studied, little is known about the thermal stability of nanocomposites. This property becomes particularly relevant since most of the composite materials used in aerospace applications are exposed to air at elevated temperature for prolonged periods. To date, the thermal stability of epoxy nanocomposites has only been investigated for model

epoxy resin (DGEBA system). These studies have reported an improvement in thermal stability of polymeric resin with addition of layered silicate (23-24). The mechanism of the improvement of thermal stability in polymer nanocomposites however is not fully understood. It is widely believed that at high temperature the amine grafted organic polymer layer will degrade from the clay particle surface resulting in more hydrophilic and less compatible clay aggregates dispersed in epoxy resin.

Thermo-gravimetric analysis (TGA)–MS studies of organo layered silicate showed that the onset temperature for decomposition of organic modifer can range from 150°C to 220°C (25). If the organically modified clay filled nanocomposites are exposed to temperatures exceeding the decomposition temperature of organic modifier, the ammonium ions are capable of undergoing thermal dissociation to generate primary amines and protons. These protons can subsequently participate in the homopolymerization of epoxies (26). The free amines can possibly react with the epoxide functionalities present inside the galleries or may diffuse out of clay particles and react with the epoxide functionalities in the bulk epoxy (27). Because these amines are primary amines, the epoxy-primary amine reactions will yield only linear cured epoxy chains unlike the conventional three dimensional cured epoxy resin. Furthermore, the epoxy-primary amine reactions can create a stoichiometric imbalance to result in the plasticization of the epoxy networks because of excess primary amine (11). Finally, the release of organic modifier from layered silicate at elevated temperature can have strong implications on the distribution of nanoclay platelets, interfacial properties, and on the ultimate mechanical properties of nanocomposite. Thus, the success of high performance nanocomposites depends on the stability of organic modifier used in the functionalization of clay as the organic treatment is the interface between layered silicate and polymer. A poor interface between polymer and layered silicate will often result in a microcomposite, or a traditional filled system. In this research, two aspects were focused : One is to make layered organosilicate with higher thermal stability. Another is to make a layered organosilicate with potential interfacial bonding between the nanosilicate and polymer matrix. Two approaches to formulate layered organosilicates nanocomposites with higher thermal stability were studied and have been discussed below.

I) Synthesis of Silylated Apophyllite Nanocomposite

In this research, apophyllite, a pure, natural and commercially-available layered silicate, was first treated with 7-octenyltrichlorosilane in order to chemically graft the functional pendent organic group containing a C=C bond. The double bond of the silylated chain can be further epoxidized or hydroxylated in the next step, so as to form a strong chemical bonding interface with the epoxy matrix.

a) Silylated Apophyllite

The reaction of 7-octenyl trichlorosilane with apophyllite has been tried and was successful. The resultant powder feels soft, which is totally different from the original apophyllite silicate crystal particles. WAXD of the apophyllite and octenylsiloxy-apophyllite was taken in a Rigaku x-ray powder diffractometer (Cu K_α radiation, generator power of 40 kV and 150 mA) with a 2θ scan range from 2.2° to 40°, and is shown in Figure 1. The x-ray diffraction clearly indicates that the three-dimensional crystal structure of the original silicate is destroyed. However, the ordered layered structure is still preserved with the 21.8 Å-interplanar spacing between the nanolayers. The original interplanar spacing between the silicate nanolayers is 7.8 Å. The gallery is expanded because of the presence of the organic pendent group inside the gallery. This supports the theory that the octenylsiloxy group has been grafted onto the silicate nanolayer backbone.

FTIR spectroscopy of the apophyllite and octenylsiloxy apophyllite was taken in a Nicolet Magna-IR 560 spectrometer and is shown in Figure 2. The Si-O-Si stretch band is very intense. The spectra from 3160 to 2760 cm^{-1} were inserted inside the complete spectral plot to show this region more clearly. The presence of the C-H band (3080 cm^{-1}) from C=C-H and C-H band (2930, 2860 cm^{-1}) from the saturated alkyl chain clearly demonstrates that the octenyl group is present in the product after the treatment of apophyllite with the 7-octenyltricholorosilane. So both x-ray diffraction and FTIR indicate that the 7-octenylksiloxy group has been successful grafted onto the backbone of apophyllite silicate sheet backbone.

TGA was used to find the thermal stability of siloxylated apophyllite powder. Thermal analysis was performed on a TA Instruments Hi-Res TGA 2950 thermogravity analyzer at 2°C/min. with nitrogen sweep gas. The TGA data are shown in Figure 3.

decomposition temperature, which is generally defined as the temperature when 5% weight is lost, is ~430°C. This decomposition temperature is much higher than that of the general organoclays, such as I.30E (~270°C). The reason for the much higher thermal stability for the octenylsiloxy-apophyllite than the general organoclays is the different decomposition temperature of the organic pendent group bonding to the silicate nanolayers. The bonding between the organic pendent group and the silicate nanolayer backbone in the octenylsiloxy-apophyllite is covalent bonding, while the bonding in the general organoclays such as I.30E is ionic bonding. The covalent bonding is much stronger than that of the ionic bonding. Therefore the octenylsiloxy-apophyllite is much more stable than the general organoclays. It must be noted that general organoclays have ionic interactions between the organic pendent group and the silicate nanolayer backbone. This result is very significant. It also opens the door for the high-temperature thermoset materials, such as bismaleimide (BMI) and polyimide, in the application of nanocomposite materials, while general organooclay cannot stand the high temperature. In addition, the introduction of the functional bonding (C=C) group, which has such a rich chemistry, makes it possible to transfer the olefinic group into the OH, epoxy group, and other functional group, and eventually be involved in forming a strong interface with the polymer matrix.

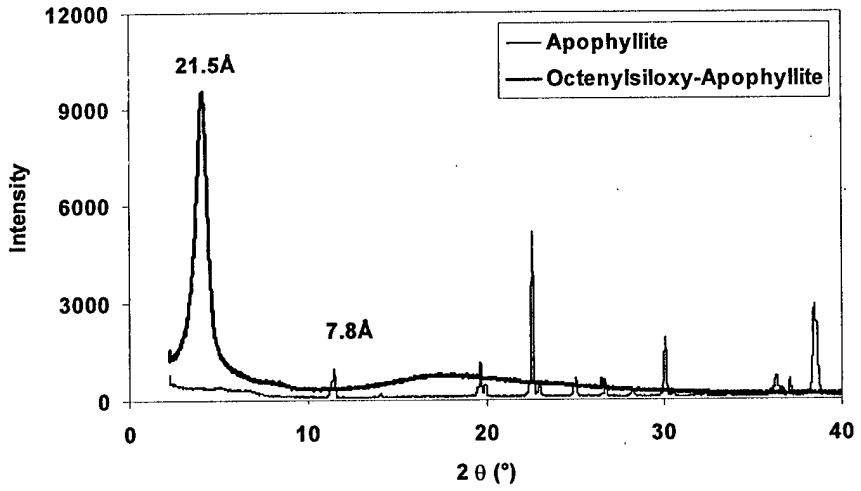

Figure 1. Wide-Angle X-ray Diffraction of the Apophyllite and 7-Octenylsiloxy-Apophyllite.

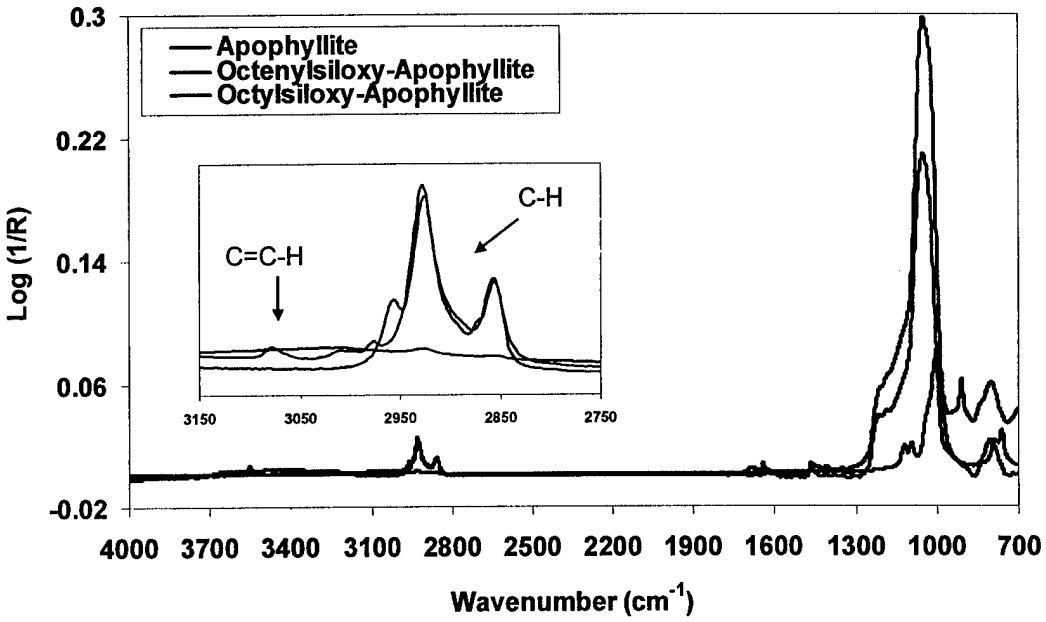

Figure 2. FTIR Spectra of the Apophyllite, 7-Octenylsiloxy-Apophyllite, and Octylsiloxy –Apophyllite.

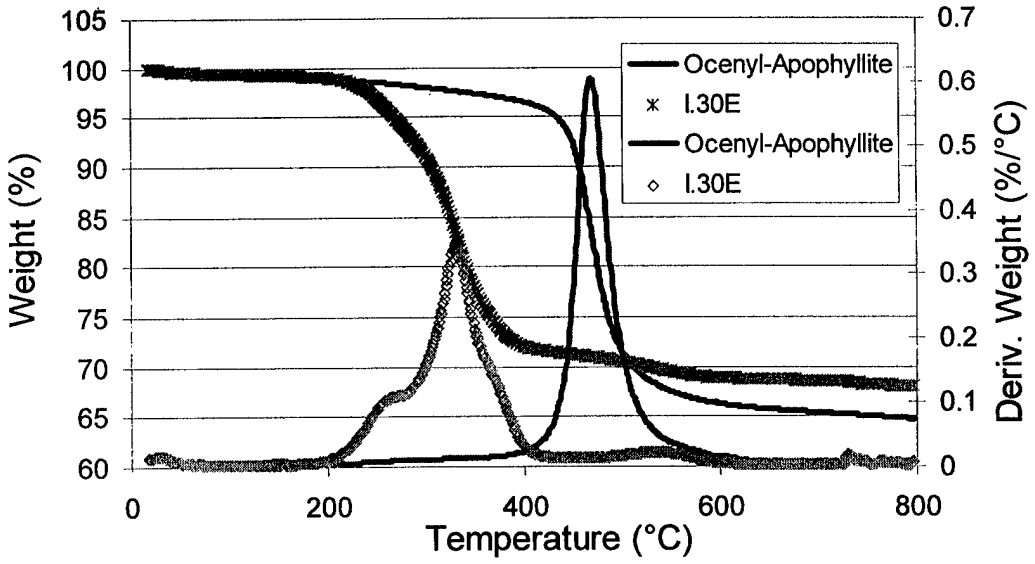

Figure 3. TGA Spectrum of the Octenylsiloxy-Apophyllite and I.30E (general commercially-available organoclay) under Nitrogen at 2°C/min.

In order to test the role of the interfacial interaction between the silicate nanolayers and polymer matrix, we attempted to synthesize a layered organosilicate with high thermal stability but without a functional group in contrast to a layered organosilicate with a functional group (such as C=C) for potential stronger interfacial bonding. The layered silicate of apophyllite was treated with *n*-octyltrichlorosilane in order to chemically graft the pendent organic group containing an inert *n*-octyl group. The covalent bond grafting guarantees higher thermal stability, while the inert *n*-octyl group makes the comparison between the strong interfacial bonding or just van der Waals interfacial interaction. The reaction was successful. The resultant powder feels soft. WAXD of the apophyllite and *n*-octylsiloxy apophyllite was taken and is shown in Figure 4. While the three-dimensional crystal structure of the original silicate is destroyed, the ordered layered structure is still preserved with the ~21.0 Å-interplanar spacing between the nanolayers. The original interplanar spacing between the silicate nanolayers is 7.8 Å. The gallery is expanded because of the presence of the organic pendent group inside the gallery. This provides the supporting evidence that the octylsiloxy group was successfully grafted onto the silicate nanolayer backbone.

FTIR spectroscopy of the apophyllite and *n*-octylsiloxy apophyllite was taken and is shown in Figure 2. The Si-O-Si stretch band is very, very intense. So the spectra from 3160 to 2760 cm^{-1} were inserted inside in order to show it more clearly. The presence of a C-H band (2960, 2930, 2860 cm^{-1}) from the saturated alkyl chain clearly demonstrates the presence of the *n*-octyl group in the product after treatment of apophyllite with the octyltricholorosilane. In comparison with the spectrum of 7-octenylsiloxy-apophyllite in Figure 2, there is no presence of the C-H band (~3080 cm^{-1}) from C=C-H in the octylsiloxy-apophyllite. So both x-ray diffraction and FTIR indicate the successful graft of the *n*-octyl group onto the layered silicate backbone.

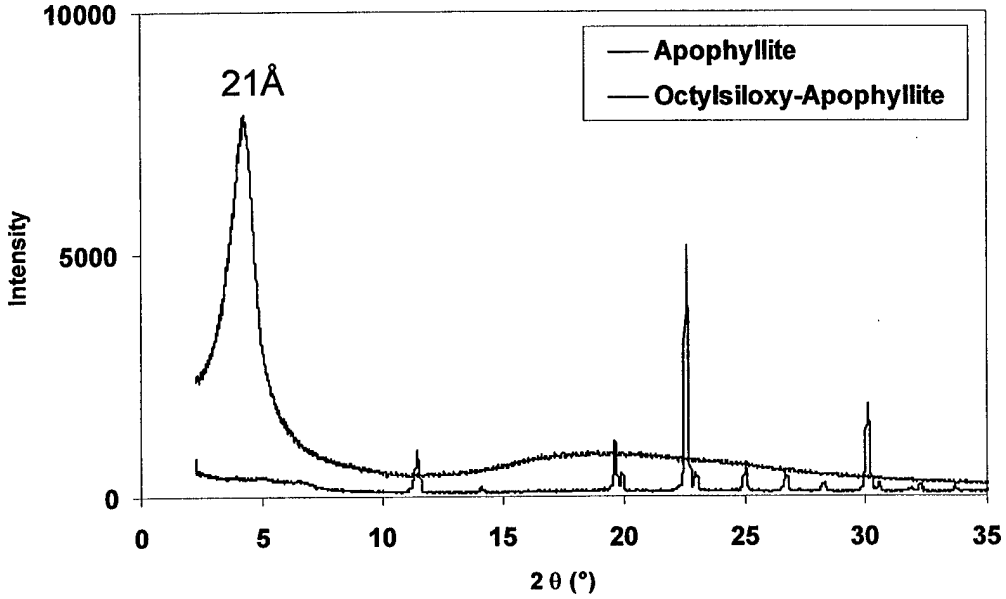

Figure 4. Wide-angle x-ray diffraction of Apophyllite and *n*-octylsiloxy-Apophyllite.

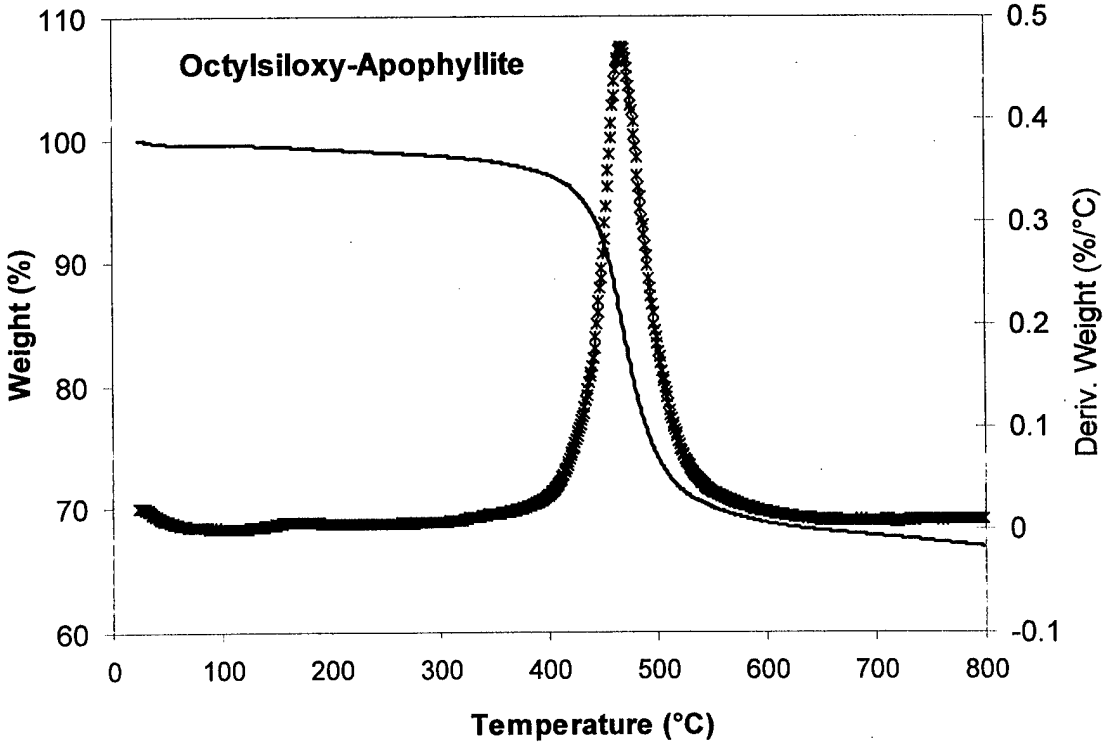

Figure 5. TGA Spectrum of the *n*-octylsiloxy-Apophyllite under Nitrogen at 2°C/min.

TGA was again used to verify the thermal stability of the octylsiloxy-apophyllite in order to show the octylysiloxy was covalently-grafted onto the backbone of the apophyllite silicate. The TGA data of the octylsiloxy-apophyllite are shown in Figure 5. The decomposition temperature is ~433°C, which indicates that this layered organosilicate is higher thermally stable than the general organoclays such as I.30E. This provides the supporting evidence of the covalent bonding between the octylsiloxy group and the silicate sheet backbone. The residue of the sample at 800°C is 67%. This indicates the substitution of the octylsiloxy group is pretty good.

b) Apophyllite Nanocomposite

The 7-octenylsiloxy apophyllite with higher thermal stability and the potential to form strong interfacial bonding with vinylic polymer was used for preparing vinylester nanocomposite. The clay was soaked in styrene while vinyl ester resin was separately soaked in styrene for 24 h. After soaking the clay and resin in styrene, both clay and resin were combined and sonified using a high power sonicator and cured using methyl ethyl ketone peroxide. Wide angle x-ray diffraction of the apophyllite clay powder and apophyllite clay vinyl ester nanocomposite was taken and is shown in Figure 6. After addition and curing of the vinyl ester resin, a new peak at $2\theta = 2.8°$ is observed that corresponds to intercalated clay platelet distribution in polymer matrix. The x-ray diffraction of this nanocomposite shows that the interplanar spacing was ~ 32 Å, which is an ~10 Å increase compared to the spacing in apophyllite clay powder ~21.5 Å. This result indicates that this new layered organosilicate is compatible with the vinyl ester, and an intercalated nanocomposite is formed. The interlayer spacing between the silicate layers in siloxylated apophyllite is somewhat expanded because of the intercalation of polymer chains inside the gallery. It must be noted that the intensity of the intercalant peak is much smaller compared to the functionalized clay particle.

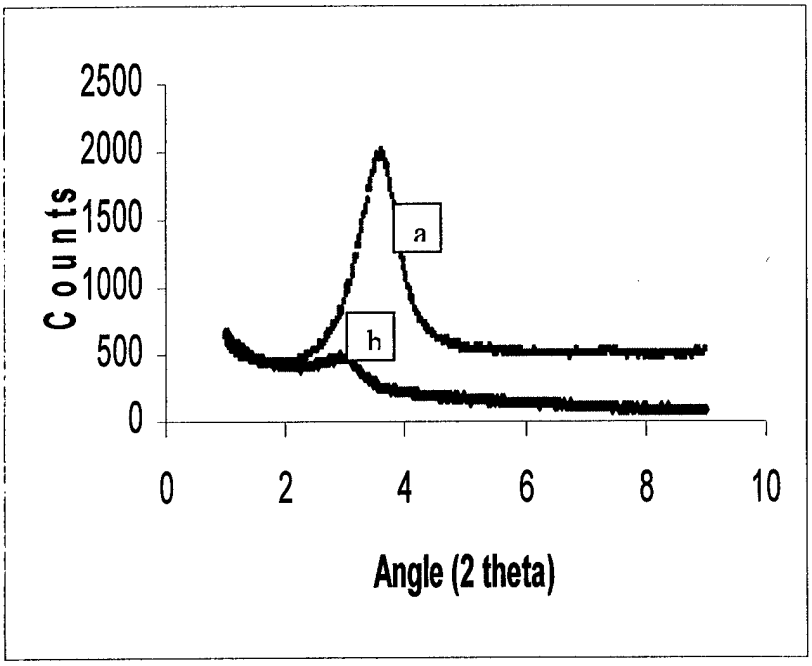

Figure 6. Wide-Angle X-ray Diffraction of (a) 7-octenylsiloxy-apophyllite and (b) 7-octenylsiloxy-apophyllite vinyl ester nanocomposite.

TEM micrograph of the octenylsiloxy apophyllite nanocomposite is shown in Figure 7. TEM micrographs of the well mixed octenylsiloxy apophyllite clay filled vinyl ester nanocomposite showed mixed bag morphology. We notice some clay aggregates, some separated clay platelets maintaining their original registery, and some clay platelets well separated and distributed in the polymer matrix. High power sonication improves dispersion of clay platelets. Most of the separated clay sheets are not observed as edge on, instead they appear as ribbons. XRD results and TEM data indicate that octenylsiloxy apophylite clay is reasonably well dispersed in vinyl ester matrix. Work is underway to achieve better clay platelet separation in apophyllite clay filled vinyl ester nanocomposite.

c) Mechanical Data of Vinyl Ester Nanocomposites:

Figure 8 compares the modulus and strength of vinyl ester nanocomposites formulated with 7-octenylsiloxy-apophyllite, n-octylsiloxy-apophyllite, and pristine vinyl ester resin. It was found that the modulus of clay filled nanocomposite is generally higher than that of pristine resin. On the other hand, the tensile strain of vinyl ester resin

decreases with addition of clay. The decrease in tensile strain of vinyl ester resin is some what expected because clay is an extremely stiff material and the addition of stiffer clay to stiff polymer matrix results in a brittle polymeric material. However, we observed that the drop in tensile strain for 7 octenyl siloxy functionalized clay filled vinyl ester is some what less than that of n-octyl siloxy functionalized clay filled vinyl ester. We consistently noticed this trend in all the nanocomposites measured. We believe that the improvement in mechanical properties of 7 octenyl siloxy functionalized clay filled vinyl ester (potential for 7-octenyl group to be directly involved in bonding with the vinylic group of the vinyl ester resin and/or styrene diluent) can probably be attributed to improved clay dispersion and clay/matrix adhesion. Further studies will be conducted to quantify the improvement in ductility of vinyl ester resin when clay with terminal bonding groups is added instead of clay with terminal non bonding groups.

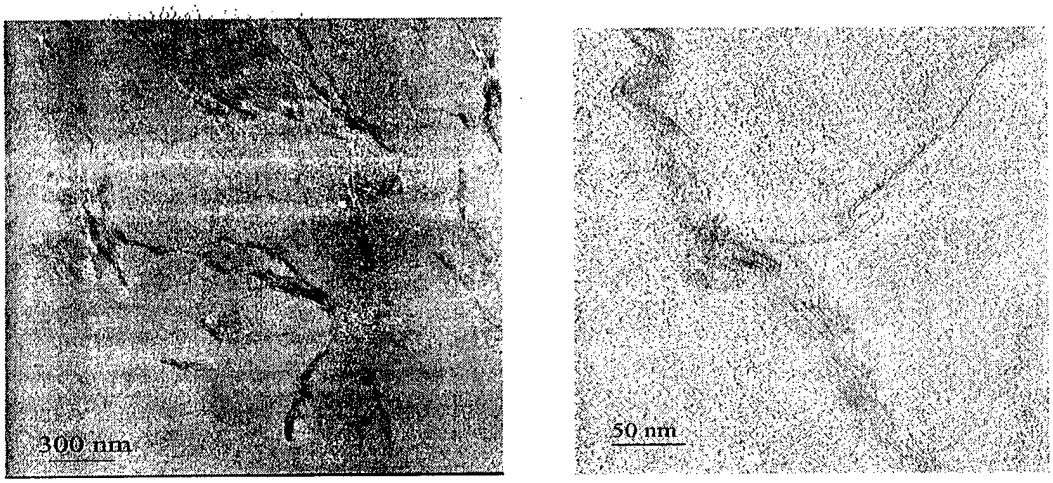

(a) (b)

Figure 7. TEM images of vinyl ester nanocomposite. (a) and (b) are the low and high magnification images of 7 octenyl apophyllite clay vinyl ester sample.

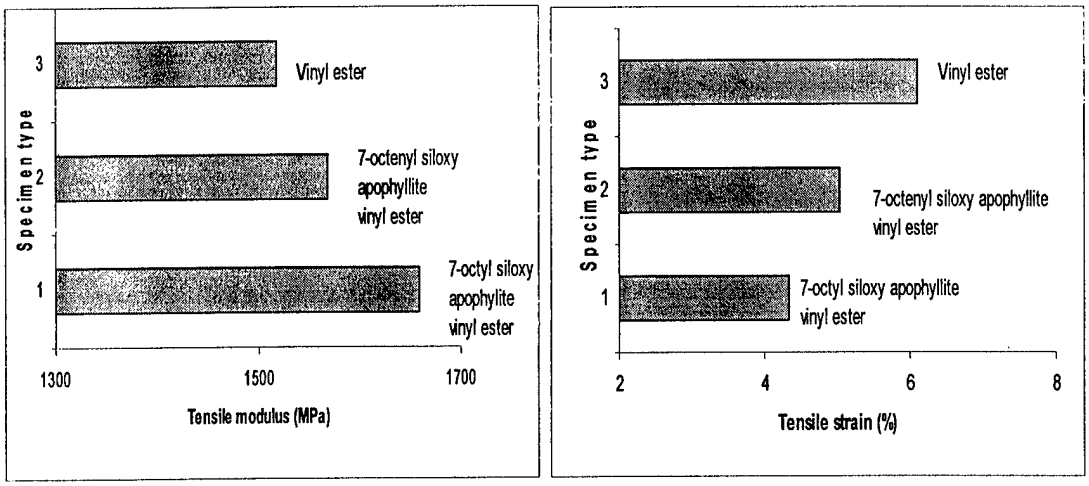

Figure 8 : Mechanical data of vinyl ester, 7 octenyl siloxy apophyllite vinyl ester, and n-octyl siloxy apophyllite vinyl ester specimen.

II) Synthesis of Imidazolium Clay Nanocomposite

In this research, commercially available natural clay was treated with a number of thermally stable imidazolium salts. Figure 9 provides the reaction sequences used in the synthesis of 1-hexadecyl-2-methyl imidazolium chloride (HDMIM) and 1-hexadecyl-3-(10-hydroxydecyl)-2-methyl imidazolium chloride (HDMHDIM) from 2- methyl imidazole. Details about the synthesis of imidazolium salts are below:

(a) Synthesis of Imidazolium Salts

Synthesis of 1-hexadecyl-2-methyl imidazole:

In a dry three necked 50 ml round bottom flask equipped with a magnetic stir bar, 2.34 g (0.06 mol) of sodium hydride (60 % NaH dispersion in mineral oil) was placed. To remove the mineral oil, petroleum ether was added, the mixture was stirred and allowed to settle and the petroleum ether was removed by pipet. A second portion of petroleum ether was added and the process was repeated. Then 5.06 g (0.06 mol) of 2-methylimidazole and 10 ml of dry THF was gradually added into the flask containing and stirred for 1.0 h. Then 9.30 mL (0.03 mol) of 1-bromohexadecane was added into the flask and the resulting mixture was stirred for 24 h at room temperature. After 24 h, unreacted sodium hydride was decomposed by adding 10 ml of saturated $NaHCO_3$ solution. To avoid any vigorous reaction, $NaHCO_3$ solution was gradually added to the

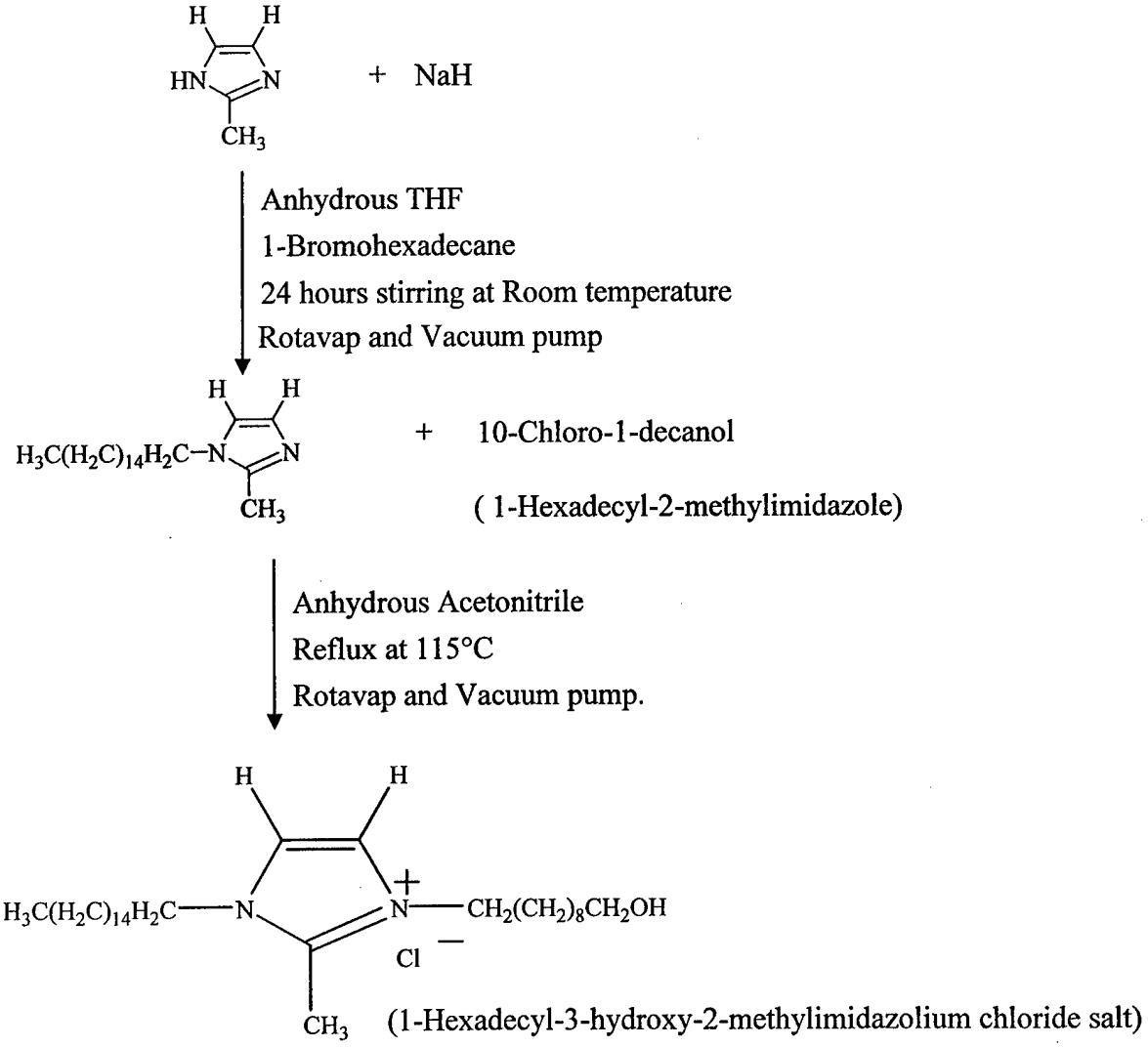

Figure 9 Reaction scheme for synthesizing 1-hexadecyl-2-methyl imidazolium chloride and 1-hexadecyl-3-(10-hydroxydecyl)-2-methyl imidazolium chloride from 2 methyl imidazole.

mixture in the flask over duration of 30 minutes. The resulting solution was then transferred into 125 mL separatory funnel and an additional 60 mL of $NaHCO_3$ solution was added. The solution was extracted three times with petroleum ether and the petroleum ether extract layers were combined and dried overnight using anhydrous magnesium sulfate. The mixture was filtered and the filtrate was collected. The filtrate was concentrated by rotary evaporation to obtain solid product. The product was characterized by MALDI-TOF and ^1H NMR. The reaction was repeated several times and the yield of product was found to be 95%. While some of the product was protonated with HCl to form 1-hexadecyl-2-methyl imidazolium chloride (HDMIM), the remaining product was used for the synthesis of 1-hexadecyl-3-(10-hydroxydecyl)-2-methyl imidazolium chloride (HDHDMIM) .

Synthesis of 1-hexadecyl-2-methyl imidazolium chloride (HDMIM)

0.25g of 1-hexadecyl-2-methyl imidazole was dissolved in 7.5 ml ether by stirring for 30 minutes. 1.7 ml of 0.5 M HCl acid was added gradually to a stirring mixture. Upon completion of addition of HCl to the mixture, the entire mixture was stirred for additional 3h. The solid was recovered by stripping ether from the mixture using vacuum oven. The yield of product was found to be 95%.

Synthesis of 1-hexadecyl-3-(10-hydroxydecyl)-2-methyl imidazolium chloride

To a 50-ml three-necked round bottom flask equipped with a condenser and a magnetic stir bar, 0.912 g (0.003 mol) of 1-hexadecyl-2-methyl imidazole was placed. The flask was placed on a nitrogen line before adding 10 ml of anhydrous acetonitrile. Then 0.61 mL (0.003 mol) of 10-chloro-1-decanol was added drop by drop and the entire mixture was refluxed with continuous stirring at 115°C. The reaction kinetics were followed by removing aliquots from the vessel at predetermined time intervals for a period of 3 weeks. The crude product was analyzed by ^1H NMR. The final mixture was transferred in a 125 ml separatory funnel and extracted three times with petroleum ether. The sample was concentrated through rotary evaporation of the petroleum ether extract. The compound was then further purified by redissolving in 1.0 mL of water, followed by extraction with petroleum ether. The water extract and petroleum ether extract was concentrated through rotary distillation. The concentrated product was dried further by pumping for 3 h at a pressure of 0.005 mm Hg. The compound (HDHDMIM) was

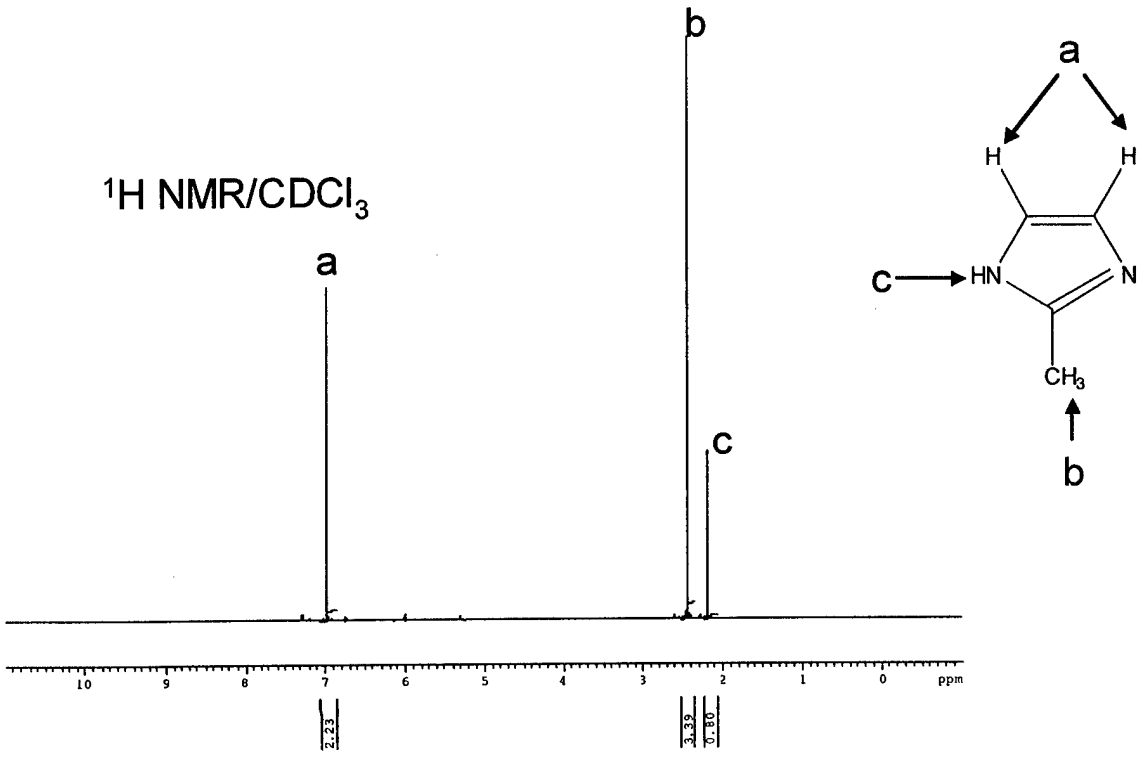
^{1}H NMR/CDCl$_3$
a
b
c
H
H
HN
N
CH$_3$
10 9 8 7 6 5 4 3 2 1 0 ppm
2.23
3.39
0.80

(a)

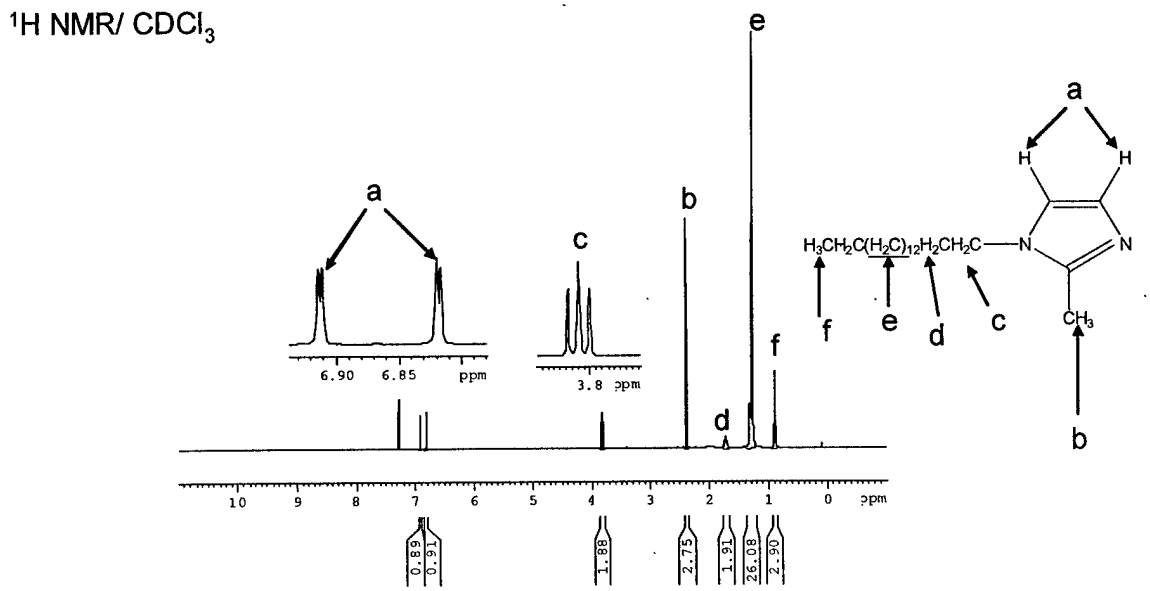
^{1}H NMR/ CDCl$_3$
a
b
c
d
e
f
6.90 6.85 ppm
3.8 ppm
H$_3$CH$_2$C(H$_2$C)$_{12}$H$_2$CH$_2$C
N
N
CH$_3$
10 9 8 7 6 5 4 3 2 1 0 ppm
0.89
0.91
1.88
2.75
1.91
26.08
2.90

(b)

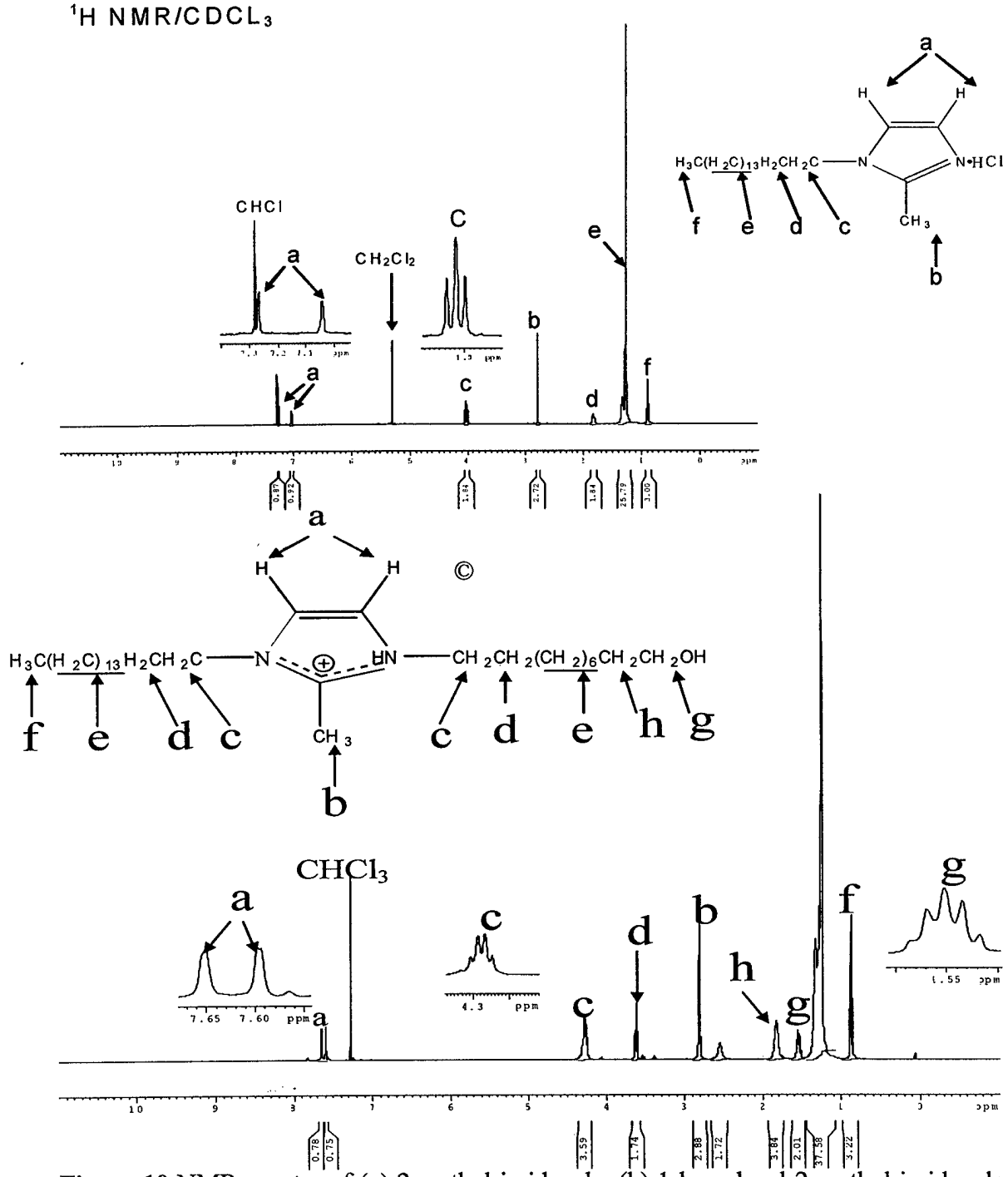

Figure 10 NMR spectra of (a) 2 methyl imidazole, (b) 1-hexadecyl-2-methyl imidazole, (c) 1-hexadecyl-2-methyl imidazolium chloride and (d) 1-hexadecyl-3-(10-hydroxydecyl)-2-methyl imidazolium chloride.

characterized by ^{1}H NMR and MALDI-TOF. The reaction was repeated several times and the yield of the final product was found to be 60 ± 5 %.

Figure 10 is the NMR spectra of the 2 methyl imidazole, 1-hexadecyl-2-methyl imidazole, 1-hexadecyl-2-methyl imidazolium chloride and 1-hexadecyl-3-(10-hydroxydecyl)-2-methyl imidazolium chloride. The ^{1}H NMR spectrum of 2-methyl imidazole had a peak at a chemical shift of 7.0 ppm, which is characteristic of the proton associated with the olefinic carbon in the starting compound. The protons associated with the olefinic carbon are not easily distinguishable, as noticed by the peak integration value. It is reasonable to assume that the proton peaks appear as a single peak because of fast chemical exchange of the NH proton between the N atoms in imidazole. We notice in the NMR spectrum of the alkylated compound, the disappearance of the peak (at 2.2 δ) corresponding to the proton associated with the N atom of 2-methyl imidazole. Further evidence for conversion of 2-methyl imidazole to hexadecyl 2-methyl imidazole is the appearance of twin olefinic proton peaks at 6.9 δ and 6.8 δ. They appear as two peaks because the environment of the olefinic proton is not similar to that observed in 2-methyl imidazole. A peak at 3.8 δ is observed that corresponds to the methylene proton adjacent to N atom of 1-hexadecyl 2-methyl imidazole. Detailed assignment of the NMR peaks can be found in Figure 10. As expected, many of the ^{1}H NMR peaks in the protonated sample of 1-hexadecyl-2-methyl imidazolium chloride appear downfield relative to the non protonated sample. The MALDI-TOF spectrum of 1-hexadecyl-2-methyl imidazolium chloride shows an intense peak at 307.54. This represents the peak corresponding to the molecular mass of protonated form of 1-hexadecyl-2-methyl imidazolium ion. Also a weak peak at m/z 531 corresponding to the di-alkylated compound ion was observed in the spectrum.

In the next step, 1-hexadecyl-2-methyl imidazole was converted to 1-hexadecyl-3-(10-hydroxydecyl)-2-methyl imidazolium chloride. The peak at ~2.5 δ is probably due to the hydroxyl proton in the 1-hexadecyl-3-(10-hydroxydecyl)-2-methyl imidazolium chloride compound. The methylene proton peak observed at 3.8 δ in the ^{1}H NMR spectra of 1-hexadecyl-2-methyl imidazole is observed in the final compound at 4.2 δ. Another methylene proton peak neighboring to the OH atom is observed at 3.5 δ, while the proton

of the OH seems to appear at 2.5 δ. The MALDI spectra of the final compound also showed the desired ion peak at m/z 463.85.

The effect of the reaction time on the N'-hydroxyalkylation of the 1-hexadecyl 2-methyl imidazole has been studied. The reaction kinetics was followed by studying the disappearance of reactant peaks at 3.8 δ for 1-hexadecyl 2-methyl imidazole and the appearance of a new methylene proton peak at 4.2 δ for 1-hexadecyl-3-(10-hydroxydecyl)-2-methyl imidazolium chloride. By using the ratio method of peak area integration, we quantified the amount of final compound formed. The peak at 0.9 δ (proton peak corresponding to methyl group) was used to normalize the peak at 3.8 δ and 4.2 δ. Figure 11 illustrates the conversion percent of starting compound and percent formation of final product at 110°C. It was observed that with extended reaction time, more conversion of reactant to product was noticed. A conversion level of about 90% is obtained in 20 days using a stoichiometric amount of the reactants.

(b) Preparation of Imidazolium Clay

Na^+-MMT (Na-montmorillonite) was provided by Southern Clay Products under the trade name of Sodium Cloisite (Na-Cloisite). Na-Cloisite has a CEC value of 92 mmole/100g clay with the exchangeable sites ionically bound with Na cations (20). Using standard cation exchange techniques sodium montmorillonite (MMT) clay was treated with Nile Blue A and a high temperature stable imidazolium-based cation, in a mass fraction ratio of 20:1. Briefly, the appropriate amount of the optical probe and HDHDMIM salt necessary to achieve complete exchange were dissolved in 50 mL of hot ethanol-water mixture. Sodium cloisite (5 g) was added with rapid stirring until the solid was well dispersed. The volume was adjusted to 100 mL with distilled water then stirred and heated for one hour at about 70°C. It was then allowed to stand in a dark cabinet for three to seven days. The exchanged clay was filtered, washed with hot 50% ethanol-water mixture, followed by 95% ethanol, until the filtrate was colorless. The washing was continued until the solid was verified for the absence of chloride ions by checking the aliquot filtrate solution with 0.1 N $AgNO_3$ solution. The resulting clay were dried at 100°C in a forced convection oven for one hour then finely ground. The clay with

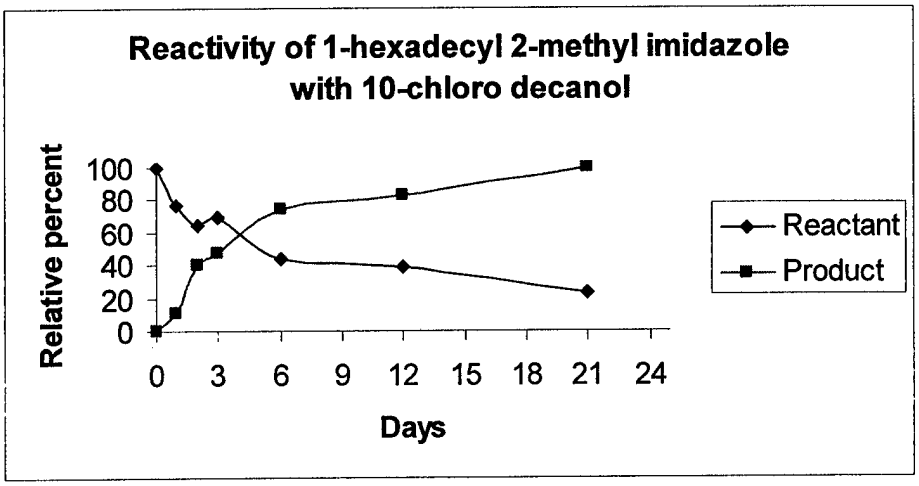

Figure 11 Percent conversion of 1-hexadecyl-2-methyl imidazole to 1-hexadecyl-3-(10-hydroxydecyl)-2-methyl imidazolium chloride with time.

HDMIM was made by following a procedure similar to that described above. The purified organo-dyed-MMT clay, designated NB-HDHDMIM-MMT, and NB-HDMIM-MMT was used for formulating nanocomposite.

(c) Formulation of Imidazolium Clay Filled Epoxy Composite

The two different organoclay were added to the epoxy resin and mixed using two different processing conditions to form nanocomposite specimen. The mixing conditions used for preparing nanocomposite samples were hand mixing and ultrasonication. For preparing epoxy nanocomposite specimens by ultrasonication, organo-dyed-MMT clay (0.3 g) was initially soaked in glycidyl methyl acrylate (1.5 g), while epoxy resin (5 g) was separately soaked in glycidyl methyl acrylate (1 g) for 24 h. After soaking the clay and resin in glycidyl methyl acrylate, both clay and resin were combined and sonicated using a high power VWR Branson Ultasonifier 250 R (frequency of 20 kHz) at 40 % duty cycle and at different output controls (from 1 to 10) for 30 minutes. During ultrasonication, the temperature of the mixture was maintained below 35^{o}C by placing the reaction vessel in an ice jacket. To the sonified mixture, 1.1 g of metaphenylene

diamine (MPDA) at 60°C was added and thoroughly mixed. The curative added mixture was poured into a silicone mold and cured at 80°C for 2 h and post cured at 110°C for 7 h in a Lab-Line Instrumentation programmable vacuum oven. The other epoxy nanocomposite specimen was prepared by hand mixing organo-dyed-MMT clay, resin, glycidyl methacrylate (GMA), MPDA mixture followed by adopting a similar curing cycle.

The nanocomposite dog-bone produced during the molding process has a fairly smooth surface. As described previously, the dog-bone specimens were cut to size and analyzed by XRD using a Scintag Inc. XRG 3000 diffractometer TEM specimens were cut from dog-bones using a Leica ultramicrotome, equipped with a diamond knife. They were collected on the surface of a water-filled trough and lifted from the surface using 200 mesh copper grids. Electron micrographs were taken with a Philips EM400T at an accelerating voltage of 120 kV.

The nanocomposite sample was characterized using an upright Laser Scanning confocal Microscope (Zeiss LSM 510). The dye doped organoclay filled epoxy samples were excited at 488 nm using Ar^+ laser light; light emitted (505 nm to 550 nm) from the sample was detected with a photomultiplier tube. Images were acquired by focusing the laser beam beneath the surface of the sample at 20 μm interval. Several images at each location along the depth of the cured film were obtained. The image acquision time was 30 s per position. The images were collected for the entire sample in few hours and this allowed to reconstruct the clay distribution in the bulk matrix.

(d) Characterization of Nanocomposite

After adding resin to clay (3.5 wt% organoclay) and hand mixing the mixture, the mixture was then cured. A peak at $2\theta = 3°$ corresponding to intercalated clay is observed along with the original peak (Figure 12). It must be noted that the peak arising from treated clay (at $2\theta = 6.3°$), remains prominent and indicates that resin intercalation in the clay gallery may have occurred to a small degree. The dark lines in the TEM micrograph of hand mixed NB-HDMIM–MMT epoxy nanocomposite correspond to MMT stacks which indicate an tactoid structure in the epoxy matrix. The clay has an average

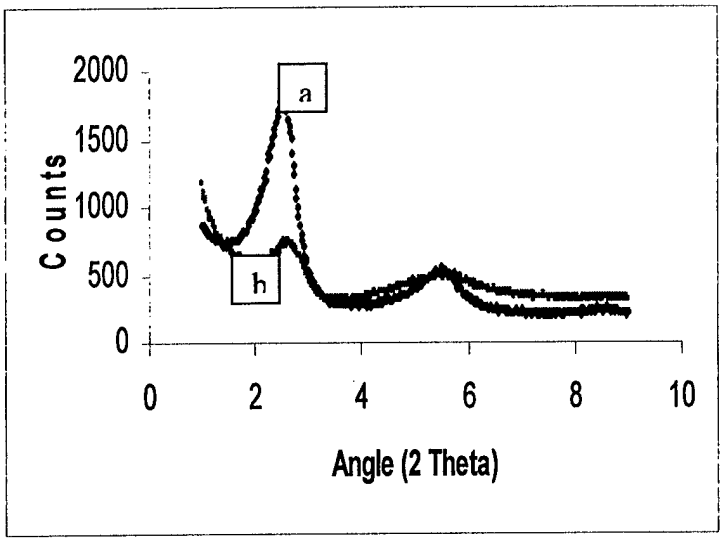

Figure 12 Wide-Angle X-ray Diffraction of (a) hand mixed and (b) ultrasonication mixed NB-HDMIM-MMT epoxy nanocomposite.

minimum layered stack thickness of 100 nm and corresponded to a minimum of 40 layers (Figure 13a and 13b).

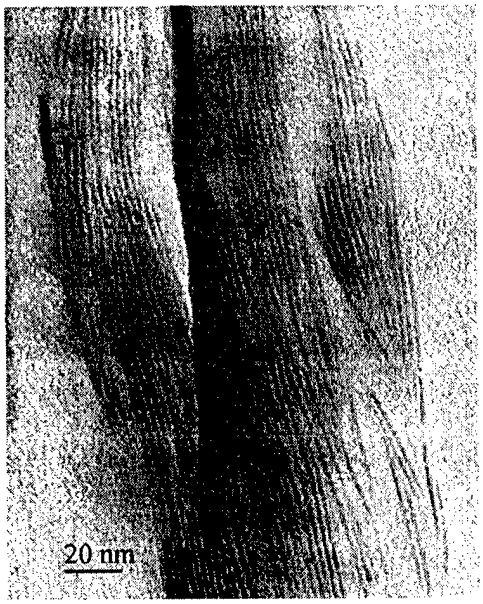

a b

Figure 13 TEM images of hand mixed NB-HDMIM-MMT epoxy nanocomposite samples. (a) and (b) are the low and high magnification images.

The role of diluent and high powered mixing on clay dispersion in epoxy matrix was evaluated. Before ultrasonication mixing, the clay and resin was soaked in glycidyl methyl acrylate, then combined and sonicated. At low magnification, the images reveal that clay is well and evenly dispersed in all nanocomposites (Figure 14a). At higher magnification, all samples exhibit dispersion of stacks of individual MMT layers that range from 2 to 10 layers in size (Figure 14b). Some individual MMT layers can be also noticed. As expected, the samples are not similar to hand mixed nanocomposite. Small clusters of micro- or nanosize in diameter of nanoclays are found along with exfoliated or intercalated nanoclay structures. The benefits of sonication in dispersing clay platelets in epoxy matrix are clearly noticeable. However, a word of caution that prolonged mixing of clay-resin mixture by sonication may result in the molecular weight reduction of polymer and/or reduction in the aspect ratio of nanoclay platelets. Therefore, the usefulness of ultrasound sonication in achieving dispersion of nanoclay platelets in polymer matrix should be carefully studied against any compromise in the mechanical properties of the nanocomposite.

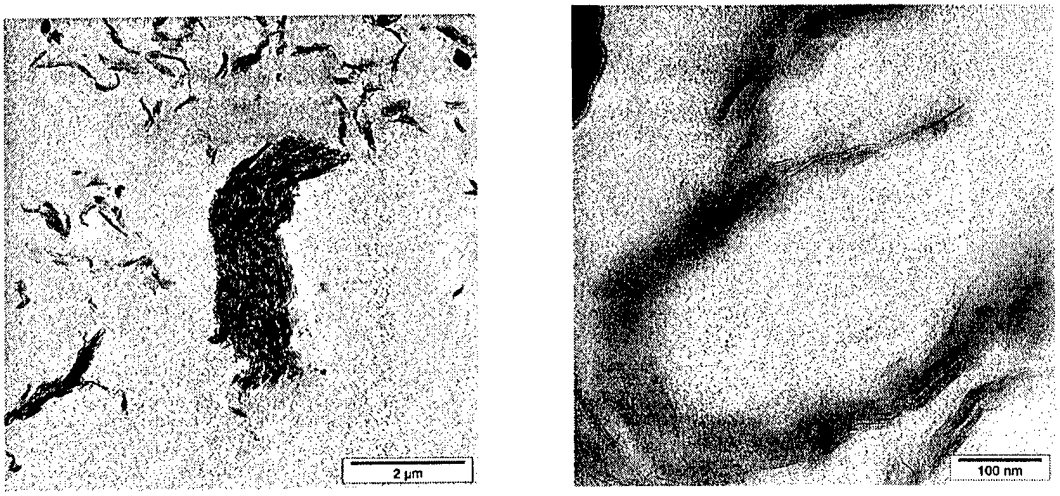

a b

Figure 14 TEM images of ultrasonication mixed NB-HDMIM-MMT epoxy nanocomposite samples. (a) and (b) are the low and high magnification images.

The XRD results are consistent with TEM observation, where the tactoid clay platelet morphology was minimally found in the sonicated sample. Unlike the hand mixed sample, the sonicated sample has shallow low angle peak at 2.25°, with d = 4.0 nm in the diffractogram and a peak at 5.45°, with d = 1.7 nm that is considerably diffused (refer Figure 12).

For deriving any quantitative information about clay platelet distribution, we estimated the platelet–neighboring platelet spacing. Our model assumes a regular, repeating lamellar structure of alternating clay and epoxy matrix. Figure 15 is the histogram representation of clay platelet separation in epoxy matrix as calculated from several TEM micrographs. The average platelet to platelet separation was found to be 4.5 nm, with some clay platelets having better separation. Generally clay platelet separation of 4.5 nm is commonly referred as intercalated morphology.

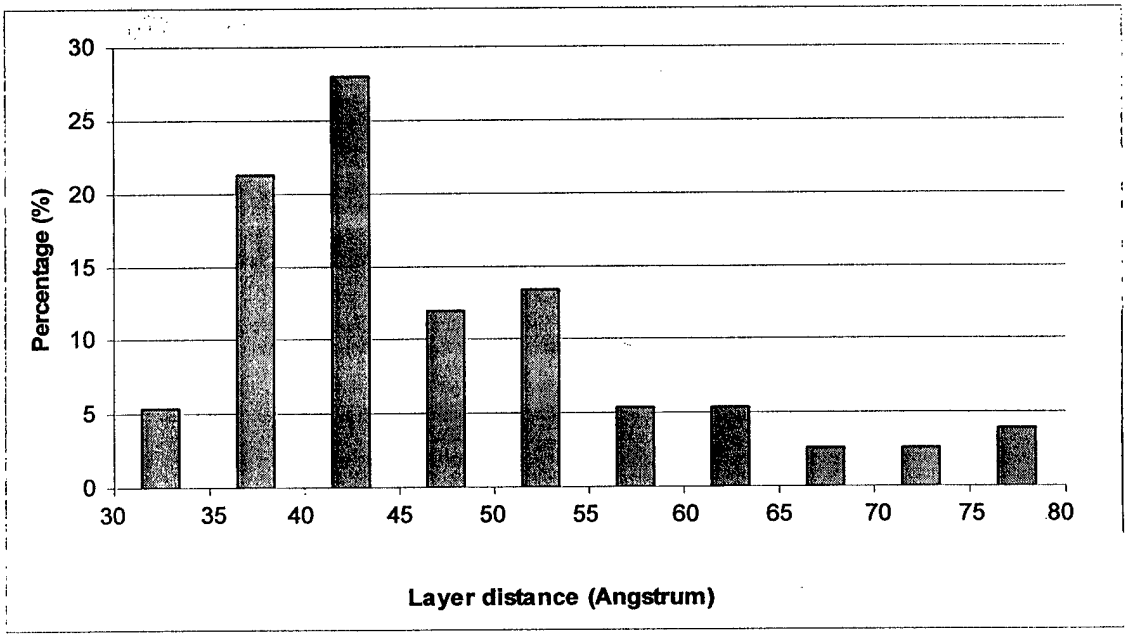

Figure 15 Histogram representation of the distribution of clay platelet separation in a ultrasonication mixed NB-HDMIM-MMT epoxy nanocomposite sample.

An attempt was made to further improve clay platelet separation in resin, by using nile blue and 1-hexadecyl-3-(10-hydroxydecyl)-2-methyl imidazolium chloride to form reactive clay instead of 1-nile blue and 1-hexadecyl-2-methyl imidazolium chloride to form nonreactive clay. The epoxy and resin mixture was mixed using sonication processing conditions. The TEM (Figure 16a) indicate that the clay platelets are uniformly distributed in the epoxy matrix. The clay platelet to neighboring clay platelet separation has improved from 4.5 nm in a sonication mixed non reactive clay nanocomposite (refer Figure 13) sample to a maximum of 7.0 nm in the sonication mixed reactive clay nanocomposite (Figure 16b).

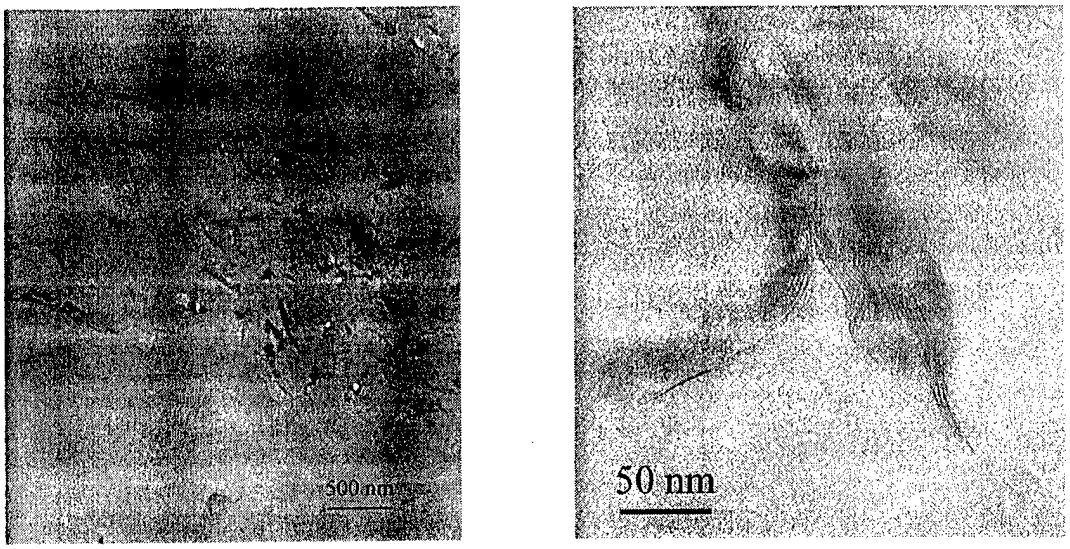

a b

Figure 16 TEM micrographs of ultrasonication mixed NB-HDHDMIM-MMT epoxy nanocomposite samples. (a) and (b) are the low and high magnification images.

The expansion of gallery spacing is believed to be because of the presence of hydroxyl functionality in imidazolium salt. The hydroxyl group of functionalized clay can assist in forming a strong chemical bond interface with the epoxy matrix. For example, the hydroxy group in the organo clay can react / favor miscibility with glycidyl methacrylate and/or epoxy resin, and/or combination thereof. Recently it was shown that

indeed vinyl functionalized-MMT bearing a styryl functional group has the strongest interaction with styrene monomer and toluene and hence the resin intercalation and exfoliation in the clay gallery is favored. The characterization of the epoxy nanocomposite to establish the coupling of imidazolium treated clay, glycidyl methyl acrylate, and/or epoxy matrix resin is a difficult and complex issue. The interface characterization is a part of an on-going investigation.

Previous work has pointed out that different tools such as TEM, and XRD may give a different picture of the state of clay platelet morphology in polymer matrix. However, some of these methods investigate only a small volume of the bulk material and/or the methodology is laborious, conclusions on the overall morphology of clay platelets in bulk should be viewed cautiously. For example, the resolution and sensitivity of X-ray scattering may not be able to pick up the presence of a small-scale intercalation and/or agglomeration of clay in the polymer matrix, while TEM can only cover only a small percent of the sample, therefore the literature results are inconclusive in showing the state of exfoliation and dispersion of clay in bulk polymer matrix. Less labor intensive characterization methods that compliment TEM and XRD characterization of polymer nanocomposites and that allows characterization over length scales in the micrometer to the submicrometer scale of the entire bulk sample would be desirable. Laser induced fluorescence spectroscopy can be studied as an alternative characterization tool to study clay dispersion in thermoset epoxy matrix because of its non-destructive nature and ease of handling. The level of clay dispersion in several epoxy nanocomposite specimens was compared and contrasted using TEM, XRD, and laser induced fluorescence spectroscopic methods.

Further characterization of the "ultrasonication mixed HDMIM-MMT" and "hand mixed HDMIM-MMT" and " ultrasonication mixed HDHDMIM-MMT" epoxy nanocomposite samples using Laser Scanning Confocal Microscopy is shown in Figure 17. Nile Blue tagged imidazolium functionalized clay particles in cured resin were studied by confocal laser microscopy. Nile Blue has an ammonium ion function, which enables some of this dye to intercalate into the clay via cation exchange reaction. Image 17a is of the hand mixed HDMIM-MMT epoxy nanocomposite sample. At laser

wavelengths of 555 nm, the Nile Blue-tagged clay which had been hand mixed for 30 minutes is observed by its emitted blue light with large diameter. Excess Nile Blue containing particles are occasionally observed as dark spots. The clay in this sample still largely exists in particulate form with some large tactoids.

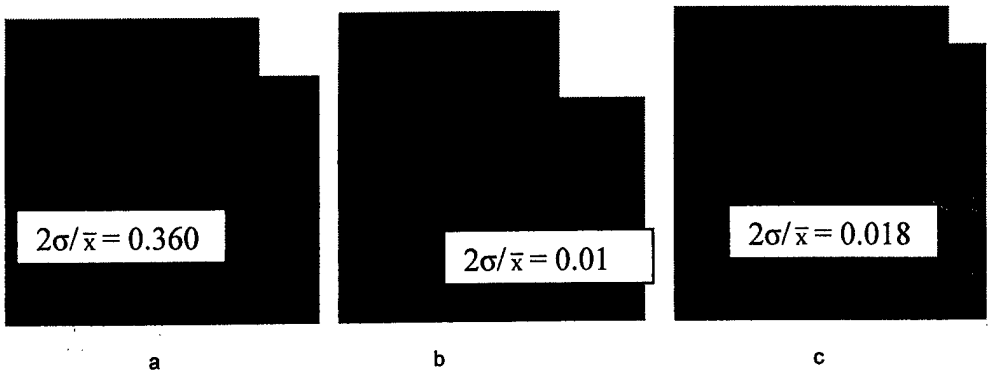

Figure 17 Orthogonal views (center=top view, top and right images are side views) of the composite-images from the confocal microscope of epoxy samples. (a) hand mixed HDMIM-MMT nanocomposite sample, (b) ultrasonication mixed HDMIM-MMT nanocomposite sample and (c) ultrasonication mixed HDHDMIM-MMT nanocomposite sample.

However, after dispersion was promoted by 30 minutes of sonication, blue emissions were occasionally seen as spots with small diameters. Figure 17b is the image of "ultrasonication mixed HDMIM-MMT" epoxy nanocomposite sample. Fluorescence labeling is one convenient method to follow the delamination process in the monomer state, during curing as well as in the cured state. The intensity of the blue light emission was sufficient to detect clay tactoids (estimate of few μm particles in the epoxy matrix). Visual inspection of the confocal images confirms the relative quality of the dispersion. Quantitative analysis of the images enables the two epoxy samples to be distinguished. Quantification was accomplished using intensity versus distance data taken along the horizontal line shown in each center-image. This gives a quantitative indication of the level of variation in the image. The mean intensity ($\bar{x}$) and the relative noise ($2\sigma/\bar{x}$) have been calculated along this line; the lower the relative noise the more homogeneous the

sample. This data is averaged over 20 lines (taken every 20 μm) using composite images made from 25 individual images (taken every 1 μm). The quantitative analysis of the confocal data shows the benefit of ultra sonication for the two epoxy samples over the hand mixing protocol.

Finally, the confocal microscopy was used to study the distribution of clay platelets on sonication mixed reactive organoclay nanocomposite. The use of reactive organoclay HDHDMIM-MMT instead of HDMIM-MMT slightly improved the final morphology of nanocomposite. The intensity of the blue light was still detectable although very small compared to that of hand mixed nanocomposite. The relative noise ($2\sigma/\bar{x}$) of the image data was small in magnitude suggesting more homogeneous distribution of the clay platelets in the sample. These results were similar in magnitude to that of sonication mixed nonreactive organoclay nanocomposite. Through these results, we demonstrate that the degree of exfoliation and dispersion of layered silicate nanocomposite is predominantly affected by processing and to a small degree by the clay chemical treatment.

The confocal results compliment TEM and XRD characterization results of polymer nanocomposites and it allows characterization over several length scales ranging from the micrometer to the nanometer scale. In addition, the confocal analysis is 3-5 times faster than TEM analysis. This approach should be applicable to characterization of other nanocomposites by using dye-tagged carbon nanotubes, nanosilicas, and polyhedral oligosilsesquioxanes (POSS).

CONCLUSIONS:

The following conclusions can be drawn from the current work:

1. The starting compound 2 methyl imidazole was treated with sodium hydride and bromohexadecane to form 1-hexadecyl-2-methylimidazole and the compound was protonated to form 1-hexadecyl-2-methylimidazolium hydrochloride (HDMIM). Subsequently, this product was reacted with chloroalcohols in anhydrous acetonitrile to obtain 1-hexadecyl-3-(10-hydroxydecyl)-2-methyl imidazolium chloride (HDHDMIM). The consumption of 1-hexadecyl-2-methylimidazole and the formation of the final product as a function of reaction time was studied. The synthesized

compound(s) were characterized by ^{1}H NMR and matrix assisted laser desorption/ionization time-of-flight mass spectrometry (MALDI-TOFMS).

2. XRD and TEM results show hand mixed nonreactive clay (HDMIM-MMT) epoxy nanocomposite exhibit tactoid morphology while ultrasonicated mixed non reactive clay exhibit highly intercalated morphology. A detailed study of the distribution of clay platelets and layer spacing in epoxy matrix indicate that on an average the interlayer spacing is 4.5 nm. TEM study of ultrasonication mixed reactive clay (HDHDMIM-MMT) epoxy nanocomposite exhibit both intercalated and exfoliated morphology. A study of the distribution of the clay platelets in epoxy matrix indicate that a maximum layer spacing of 7.0 nm can be observed.

3. Confocal microscopy was first time used to obtain mesoscale dispersion of Nile Blue tagged clay platelets in cured epoxy matrix. There was evidence of aggregated clay platelet regions in the hand mixed sample. Sonication of the sample improved the separation of clay platelets and the combined effect of sonication on reactive clay nanocomposite gave mixed morphology. Visual inspection of the confocal images confirmed the superior quality of the clay dispersion in sonicated samples as opposed to hand mixed nanocomposite samples. The positive attributes of confocal microscopy are that the clay platelet distribution through out the bulk specimen can be obtained in 3h with minimal sample preparation and is non destructive technique. Finally bulk fluorescence data was collected to study the changes in the environment of the dye molecule as it relates to clay platelet morphology in epoxy nanocomposite.

4. The layered organosilicates with higher thermal stability were synthesized by the covalent-bonding grafting chemistry. The TGA studies showed that the decomposition temperature of the organosilicate can be as high as ~430°C, much higher than the general organoclays (~250°C). The characterization from FTIR and WAXD supports that the graft is successful. In addition, two types of the higher thermally stable organosilicate with a functional group or with an inert group were made, which was designed to see the difference

between the strong interface and weak interface. All of these two layered-organosilicates were used to prepare nanocomposites with vinylic polymer. The initial study showed the intercalated nanostructure with considerable clay dispersion can be achieved. More effort is needed to make the exfoliated nanostructure. In addition, an improvement in tensile strain of vinyl ester nanocomposite was noticed when clay with terminal bonding group was used instead of clay with terminal non bonding group.

ACKNOWLEDGMENTS:

Special thank to M. Williams, J. Gilman, S. Bellayer from NIST for assisting with some of the measurements.

REFERENCES :

1. Kojima, Y., Usuki, A., Kawasumi, M., Okada, A., Fukushima, Y., Kurauchi, T. and O. Kamigaito, O. (1993). J. Mater. Res., 8: 1185-1189.
2. Messersmith, P. B., and Giannelis, E. P. (1995). J. Polym. Sci. Polym. Chem. Edn., 33: 1047-1057.
3. Kornmann, X., Berglund, L. A., Sterte, J. and Giannelis, E. P. (1998). Polym. Eng. Sci., 38(8): 1351-1358.
4. Wang, Z. and Pinnavaia, T. J. (1998). Chem. Mater., 10(12): 3769-3771.
5. Shah, A. P., Gupta, R. K., Gangarao, H. V. S. and Powell, C. E. (2002). Polym. Eng. Sci., 42(9): 1852-1858.
6. Giannelis, E. P. (1996). Adv. Mater., 8(1): 29-35.
7. Vaia,A.R. and Wagner,H.D. (2004). Materials Today, Volume 7, Issue 11:32-37 & 38-42.
8. Lagaly, G. (1999).Appl. Clay Sci.: 15, 1-9.
9. Garces, J. M., Moll, D. J., Bicerano, J., Fibiger, R. and McLeod, D. G. (2000). Adv. Mat, 12: 1835-1839.
10. Liu, W., Hoa,S.V. and Pugh, M. (2005).Composites Science and Technology, Volume 65, Issue 2:307-316.

11. Park, J.and Jana, S.C. (2004). Polymer, Volume 45, Issue 22, 13: 7673-7679.

12. Barker, O., Varley,R.J. and Simon, P.G. (2004). European Polymer Journal, Volume 40, Issue 1:187-195

13. Chen,C., Khobaib, M. and Curliss,D. (2003). Progress in Organic Coatings, Volume 47, Issues 3-4: 376-383

14. Tolle, T. B. and Anderson, P. D. (2002). Composites Science and Technology, Volume 62, Issues 7-8: 1033-1041

15. Chin, I., Thurn-Albrecht, T., Kim, H., Russel, P.T. and Wang, J. (2001). Polymer, Volume 42, Issue 13:5947-5952

16. Kornmann, X., Lindberg, H. and Berglund, A. (2001). Polymer, Volume 42, Issue 10: 4493-4499.

17. Tsai, J. and Sun, C. T. (2004). J. Compos Mater **38** (7): 567–579

18. Brown, J. M.,Curliss, D. and Vaia, R. A. (2000). *Chem Mater*, 12: 3376.

19. Zilg, C., Thomann, R., Baumert, M., Finter, J. and Mulhaupt. (2000). Macromol Rapid Commun **21,** 17: 1214–1219.

20. Ishida, H., Campbell, S., Blackwell J. (2000). Chem. Mater.12: 1260-1267

21. Fu, X., A. and Qutubuddin, S. (2005). Journal of Colloid and Interface Science, Volume 283, Issue 2: 373-379.

22. Yebassa, D., Balakrishnan, S., Feresenbet, E., Raghavan, D., Start P.R. and Hudson, S. D. (2004). J. Polym. Sci. Polym. Chem. Edn., 42:1310

23. Park, J. S., Seo, D. I. And Lee, R. J. (2002). J. Colloid Interface Sci. **251**: 160–165.

24. Zhu, J., Uhl, M.F., Morgan, B.A. and Wilkie, A. C. (2001). Chem. Mater. **13**: 4649–4654.

25. Xie, W., Gao, Z., Pan, W-P., Hunter, D., Singh, A. and Vaia, R. (2001). Chemistry of Materials, 13: 2979

26. Lan, T., Kaviratna, P. D. and Pinnavaia, J. T. (1996).J Phys Chem Solids **57**: 1005

27. Wang, S. M. and Pinnavaia, J. T. (1994). Chem Mater **6** : 468.

28. Sue, H. J., Gam, T. K., Bestaoui, N., Clearfield, A., Miyamoto, M. and Miyatake, N. (2004). Acta Materialia, Volume 52, Issue 8: 2239-2250.

29. Severe, G., Hsieh, J.A. and Koene, E. B. (2000). 58th ANTEC **2**: 1523–1526

30. Maupin, P.H.; Gilman, J.W.; Bourbigot, S.; Harris, R.H. Jr.; Bellayer, S.; Bur, A.J.; Roth, S.C.; Murariu, M.; Morgan, A.B.; Harris, J.D. (2004). Macromol. Rapid Comm, 25 (7): 788-792,

31 Ngo, H., LeCompte, K., Hargens, L. and McEwen B. A. (2000).

Thermochim Acta: 357: 97

32. Begg, G., Grimmett, R. M. and Wethey, D. P. (1977). Australian Journal of Chemistry, 30: 2005.

33 Lopez-Pestana, J. M., Diaz-Teran, J., Avila-Rey, J. M. Rojas-Cervantes, L.M. and Martin-Aranda, M. R. (2004). Microporous and Mesoporous Materials, 67: 87-94,

34 Khabnadideh, S., Rezaei, Z., Khalafi_Nezhad, A., Bahrinajafi, R., Mohamadi, R. and Farrokhroz, A. A. (2003). Bioorganic & Medicinal Chemistry Letters, Volume 13, Issue 17: 2863-2866.

35 Yoonessi, M., Toghiani, H., Kingery, L. W. and Pittman, Jr.,U. C. (2004). *Macromolecules,* **37** (7): 2511 -2518,